

Vibrational Spectra of Dipyrido[3,2-*a*:2′,3′-*c*]phenazine and Its Radical Anion Analyzed by Ab Initio Calculations and Deuteration Studies

Benjamin James Matthewson, Amar Flood, Matthew Ian James Polson, Christopher Armstrong†, David Lee Phillips††, and Keith Christopher Gordon*

University of Otago, Department of Chemistry, Union Place, Dunedin, New Zealand

†School of Chemistry, University of Sydney, NSW, 2006, Australia

††Department of Chemistry, The University of Hong Kong, Pokfulam Road, Hong Kong

(Received August 9, 2001)

The ligand dipyrido[3,2-*a*:2′,3′-*c*]phenazine (dppz) and its deuterated analogues, d_4-dppz, d_6-dppz, d_{10}-dppz, and [ReCl(CO)$_3$] complexes with these ligands have been synthesized. Using DFT calculations it is possible to calculate a geometry of the ligand such that it matches the crystallographic data for a variety of dppz complexes. B3LYP/6-31G(d) frequency calculations correspond closely to the experimental IR and Raman data. Analysis of the calculated normal modes of vibration reveals the presence of a number of modes that are localized to the ring sections of the dppz-framework. Modes 79, 78, 77, 50, and 49, which lie at 1602, 1586, 1576, 1071, and 1034 cm^{-1}, respectively, in the experimental spectra of dppz correspond to phenanthroline-based modes. Modes 68 and 67, lying at 1414 and 1402 cm^{-1} in dppz are phenazine-based vibrations. These provide an insight into the nature of the MLCT transitions for metal complexes with dppz. The preferential enhancement of phenanthroline-based modes in the resonance Raman spectra of these complexes strongly suggests the π^* accepting MO is of phenanthroline character. DFT calculations (B3LYP/6-31G(d)) on the radical anion reveal the elongation of bonds about the pyrimidine ring. The frequency calculations also reveal significant changes in the vibrational spectra for dppz$^{\bullet-}$ from the neutral ligand. Experimental resonance Raman data for the electrochemically reduced [ReCl(CO)$_3$(dppz)]$^-$ and the deuterated analogues show distinct isotope shifts that may be correlated to results obtained from the calculations. The characteristic bands observed in these spectra are phenanthroline-based. They may be correlated with time-resolved resonance Raman spectra of Ru(II) and Re(I) complexes.

Metal complexes containing the ligand dppz, and substituted analogues thereof, have received much attention because of the interaction of such complexes with DNA.[1] The intercalation of the dppz ligand between the base pairs of DNA results in a dramatic enhancement of the fluorescence of Ru(II) complexes leading to the "molecular light switch" effect.[2,3] The photophysical properties of complexes containing dppz are complicated by the presence of three close-lying excited states of LC and MLCT origin.[4] Dynamics studies on [Ru(phen)$_2$dppz]$^{2+}$ reveal an interplay between two MLCT states, termed MLCT(1) and MLCT(2), in the first few picoseconds after excitation.[5] The spectral properties of complexes containing dppz are attributed, in part, to the unoccupied MOs in the ligand. The MOs may be based over the ABC-rings (phen-based) or BDE-rings (phenazine-based) of the ligand framework (Fig. 1).[6]

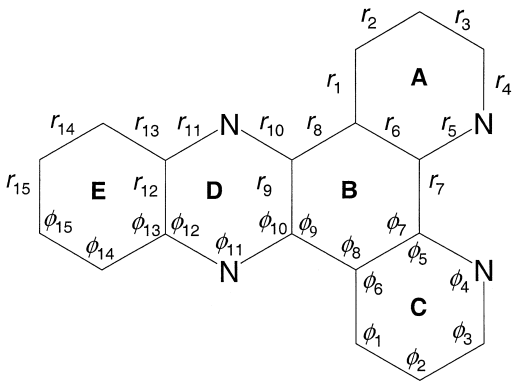

Fig. 1. Skeletal structure of dppz with bond parameters and ring labels.

Ultrafast time-resolved resonance Raman (TR^3) spectroscopy of [Ru(bpy)$_2$dppz]$^{2+}$ also reveals the presence of differing excited states as a function of solvent.[7] A number of detailed TR^3 studies have been carried out on [Ru(L)$_2$dppz]$^{2+}$ (L = 2,2′-bipyridine or 1,10-phenanthroline) and although these have provided further insight into the nature of the excited state formed by photoexcitation the findings are somewhat ambiguous and sometimes contradictory.[2,8] One of the difficulties in studying these systems is that the vibrational spectra are very complex. The number of vibrational degrees of freedom is very large, 90 modes for dppz alone. Furthermore many of the vibrational modes for dppz overlap with those of bpy or phen. This further complicates attempts to interpret vibrational data for the ground or excited states. It is possible to disentangle some of this vibrational morass by studying complexes in which only the dppz ligand contributes to the vibrational spectrum. This may be achieved in resonance Raman spectroscopy using [Cu(PPh$_3$)$_2$]$^+$ or [ReCl(CO)$_3$] moieties.[9] A fur-

ther step in elucidating the vibrational spectrum of dppz is to use computational methods to model the ligand and its spectra (IR and Raman). Studying the deuterated analogues of dppz can also aid in spectral interpretation. Such analyses have been successfully applied to other smaller polypyridyl ligands.[10] We have attempted to model the dppz ligand using ab initio computational methods and compare the results of these calculations with spectra of dppz and its deuterated analogues, in order to better understand the vibrational data. We have also studied the radical anion of dppz through the spectroelectrochemistry of the Re(I) complexes, [$ReCl(CO)_3$(dppz)]. Calculations on the radical anion provide some insight into these spectral data.

We restrict our analysis to the 1000–1650 cm^{-1} region of the spectrum because most of the spectroscopic data collected on dppz and its complexes is in that region. A further advantage of this restriction is that we only consider about 20 normal modes of vibration.

Experimental

Synthesis. Perdeuteration of aromatic species was achieved using a variation on the method of Junk et al.[11] The synthesis of dppz and its isotopomers was developed from literature methods.[12] $ReCl(CO)_5$ was prepared in accordance with reported procedures.[13] The rhenium dppz complexes were synthesised by a similar method to that of Caspar and Meyer.[14] Selectively deuterated compounds were obtained from the Schiff base reactions of perdeuterated and non-deuterated reactants.[12] For perdeuterated materials the ^1H NMR spectra show only singlets, indicating a high level of incorporation of D into the samples. For selectively deuterated samples, such as d_4-dppz, the ^1H NMR only show signals from the undeuterated sites, also indicating a high level of D incorporation.

***d*$_4$-1,2-Phenylenediamine.** Yield: 53%. ^2H NMR (DMSO) δ 6.65 (s, 2d) and 6.53 (s, 2d); MS (EI) *m*/*z* 112 (M^+). Found: C, 64.31; H, 7.21; N, 24.85%. Anal. Calcd for $C_6H_4D_4N_2$: C, 64.28; H, 7.19; N, 25.00%.

***d*$_8$-1,10-Phenanthroline.** Yield: 77%. ^2H NMR ($CHCl_3$) δ 9.25 (s, 2d), 8.29 (s, 2d), 7.81 (s, 2d), and 7.68 (s, 2d); MS (EI) *m*/*z* 188 (M^+). Found: C, 74.86; H, 4.88; N, 14.59%. Anal. Calcd for $C_{12}D_8N_2(H_2O)_{0.3}$: C, 74.44; H, 4.48; N, 14.47%.

dppz. Yield: 27%. ^1H NMR ($CDCl_3$) δ 9.69 (d, 2H, J = 9 Hz), 9.29 (d, 2H, J = 3 Hz), 8.39 (dd, 2H, J_1 = 6 Hz, J_2 = 3 Hz), 7.95 (dd, 2H, J_1 = 6 Hz, J_2 = 3 Hz), and 7.82 (dd, 2H, J_1 = 9 Hz, J_2 = 3 Hz).

***d*$_4$-dppz.** Yield: 77%. ^1H NMR ($CDCl_3$) δ 9.68 (d, 2H, J = 6 Hz), 9.29 (d, 2H, J = 6 Hz), and 7.82 (dd, 2H, J_1 = 6 Hz, J_2 = 3 Hz); ^2H NMR ($CHCl_3$) δ 8.41 (s, 2d) and 7.98 (s, 2d).

***d*$_6$-dppz.** Yield: 86%. ^1H NMR ($CDCl_3$) δ 8.38 (dd, 2H, J_1 = 9 Hz, J_2 = 3 Hz), and 7.94 (dd, 2H, J_1 = 6 Hz, J_2 = 3 Hz); ^2H NMR ($CHCl_3$) δ 9.71(s, 2d), 9.31 (s, 2d) and 7.85 (s, 2d).

***d*$_{10}$-dppz.** Yield: 75%. ^2H NMR ($CHCl_3$) δ 9.72 (s, 2d), 9.34 (s, 2d), 8.33 (s, 2d), 8.00 (s, 2d), and 7.88 (s, 2d).

[Re(I)Cl(CO)$_3$ (dppz)]. Yield: 79%. ^1H NMR ($CDCl_3$) δ 9.88 (d, 2H, J = 9 Hz), 9.48 (d, 2H, J = 6 Hz), 8.47 (dd, 2H, J_1 = 6 Hz, J_2 = 3 Hz), 8.08 (dd, 2H, J_1 = 6 Hz, J_2 = 3 Hz), and 8.04 (dd, 2H, J_1 = 9 Hz, J_2 = 6 Hz); MS (ES) *m*/*z* 594 (M–Cl + CH_3CN). Found: C, 42.21; H, 1.74; N, 9.20%. Anal. Calcd for $C_{21}H_{10}ClN_4O_3Re(CH_2Cl_2)_{0.25}$: C, 41.89; H, 1.84; N, 9.31%.

[Re(I)Cl(CO)$_3$(*d*$_4$-dppz)]. Yield: 65%. ^1H NMR ($CDCl_3$) δ 9.88 (d, 2H, J = 9 Hz), 9.48 (d, 2H, J = 6 Hz), and 8.04 (dd, 2H, J_1 = 9 Hz, J_2 = 6 Hz); ^2H NMR ($CHCl_3$) δ 8.52 (s,2d) and 8.13 (s,2d); MS (ES) *m*/*z* 598 (M–Cl + CH_3CN). Found: C, 40.76; H, 1.51; N, 8.72%. Anal. Calcd for $C_{21}H_6D_4ClN_4O_3Re(CH_2Cl_2)_{0.50}$: C, 40.70; H, 1.75; N, 8.83%.

[Re(I)Cl(CO)$_3$(*d*$_6$-dppz)]. Yield: 57%. ^1H NMR ($CDCl_3$) δ 8.47 (dd, 2H, J_1 = 6 Hz, J_2 = 3 Hz) and 8.08 (dd, 2H, J_1 = 6 Hz, J_2 = 3 Hz); ^2H NMR ($CHCl_3$) δ 9.93 (s,2d), 9.51 (s,2d), and 8.08 (s,2d); MS (ES) *m*/*z* 600 (M–Cl + CH_3CN). Found: C, 42.43; H, 1.68; N, 9.32%. Anal. Calcd for $C_{21}H_4D_6ClN_4O_3Re$: C, 42.47; H, 1.70; N, 9.44%.

[Re(I)Cl(CO)$_3$(*d*$_{10}$-dppz)]. Yield: 61%. ^2H NMR ($CHCl_3$) δ 9.94 (s,2d), 9.52 (s,2d), 8.52 (s,2d), and 8.10 (s,4d); MS (ES) *m*/*z* 604 (M–Cl + CH_3CN). Found: C, 42.88; H, 1.82; N, 9.51%. Anal. Calcd for $C_{21}D_{10}ClN_4O_3Re$: C, 42.18; H, 1.69; N, 9.37%.

Spectral Measurements. ^1H and ^2H NMR spectra were recorded on a Varian ^{UNITY}Inova-300 2 Channel FT 300 MHz or a Varian ^{UNITY}Inova-500 2 Channel FT 500 MHz spectrometer. The chemical shift values reported were calibrated with residual solvent signals. Mass spectrometry measurements were obtained from either a MS80RFA for (EI) or a Micromass LCT instrument for electrospray (ES) measurements.

FTIR spectra were collected using a Perkin Elmer Spectrum BX FT-IR system on sample solutions ($CDCl_3$) contained in a transmission cell (0.5 mm pathlength) with CaF_2 windows. FT-Raman spectra were collected on powder samples using a system previously described.[15] Resonance Raman spectra, generated with continuous wave excitation, were obtained using an air-cooled argon ion laser (Melles-Griot Omnichrome 543-MAP). Plasma emission lines were removed from the exciting beam using bandpass filters or a wavelength specific holographic laser bandpass filter (Kaiser Optical Systems Inc.). Typically the laser output was adjusted to give 25 mW at the sample. The incident beam and the collection lens were arranged in a 135° back-scattering geometry to reduce Raman intensity reduction by self-absorption.[16] An aperture-matched lens was used to focus scattered light through a narrow band line-rejection (notch) filter (Kaiser Optical Systems) and a quartz wedge (Spex) and onto the entrance slit of a spectrograph (Spex 750M). The collected light was dispersed in the horizontal plane by a 1800 grooves/mm holographic diffraction grating and detected by a liquid nitrogen cooled 1152-EUV CCD controlled by a ST-130 controller and CSMA 2.3b(v.2) software (Princeton Instruments). Spectra were analysed using GRAMS 5.0 (Galactic Industries). The cell used for Raman spectroelectrochemistry was an OTTLE cell of our own design.[17]

Computational Methods. The vibrational frequencies and their IR and Raman intensities were calculated using DFT calculations (B3LYP functional, 6-31G(d) basis set). These were implemented with the Gaussian 98[18] and 94[19] program packages. The visualization of the MOs and vibrational modes was provided by the Molden package.[20]

Results and Discussion

The dppz ligands are generally only partially soluble in most solvents (ca 30 mmol L^{-1} in $CHCl_3$). They are emissive under laser radiation in the visible and Raman spectra can only be obtained with NIR excitation.

Neutral Ligand: Spectra and Calculations. In describing the structural characteristics of the dppz ligand we have adopted a labelling system. This is shown in Fig. 1.

The calculated structural parameters for dppz are presented

Table 1. Bond Lengths and Angles Calculated Using Ab Initio Methods and from Selected Crystal Structures

Bond parameters[a]	dppz HF[b] 3-21G[c]	dppz HF 6-31G(d)	dppz B3LYP 6-31G(d)	**1**[d]	**2**[e]	$dppz^{\bullet-}$ B3LYP 6-31G(d)
r_1	1.393	1.398	1.406	1.423	1.377	1.413
r_2	1.373	1.37	1.383	1.347	1.387	1.38
r_3	1.390	1.395	1.404	1.389	1.380	1.41
r_4	1.320	1.307	1.327	1.347	1.338	1.324
r_5	1.332	1.330	1.347	1.328	1.361	1.354
r_6	1.392	1.395	1.415	1.441	1.371	1.428
r_7	1.471	1.481	1.476	1.473	1.431	1.457
r_8	1.458	1.467	1.462	1.441	1.462	1.452
r_9	1.423	1.432	1.439	1.46	1.408	1.421
r_{10}	1.306	1.299	1.327	1.311	1.315	1.353
r_{11}	1.352	1.342	1.353	1.323	1.370	1.367
r_{12}	1.403	1.407	1.435	1.435	1.429	1.441
r_{13}	1.415	1.421	1.421	1.426	1.430	1.412
r_{14}	1.354	1.356	1.375	1.345	1.365	1.393
r_{15}	1.422	1.423	1.422	1.439	1.399	1.403
ϕ_1	119.3	119	119.1	119.2	120.2	119.7
ϕ_2	118.3	118	118.2	123.2	119.0	118.3
ϕ_3	122.6	123.7	124.0	121.8	122.4	123.9
ϕ_4	119.8	118.8	118.2	116.7	118.1	118.4
ϕ_5	118.6	118.1	122.3	123.4	122.8	122.4
ϕ_6	118.6	118.1	118.2	118.7	117.4	117.4
ϕ_7	119.8	119.9	119.8	118	120.1	118.8
ϕ_8	120.8	120.7	120.7	119.7	118.9	122.1
ϕ_9	119.4	119.4	119.6	120.6	120.4	119.1
ϕ_{10}	120.5	121.1	124.5	120.2	122.3	122.4
ϕ_{11}	119.7	118.3	117.7	118.8	117.3	116
ϕ_{12}	119.8	120.6	120.9	121.4	121.6	121.5
ϕ_{13}	119.6	119.5	119.3	117.5	118.7	118.7
ϕ_{14}	119.7	119.9	120.0	120.3	120.8	121.3
ϕ_{15}	120.6	120.7	120.7	120.9	119.4	120

a) Bond lengths (r)/Å, bond angles (ϕ)/degrees. Labels are given in Fig. 1.
b) Ab initio method used.
c) Basis set used in calculation of geometry.
d) Ligand crystal structure from Ref. 21.
e) Ligand crystal structure from Ref. 22.

in Table 1 along with the observed parameters for a number of single crystal structures of the ligand bound to metals. The calculated structure for dppz (B3LYP/6-31G(d)) shows the C–C bonds of ring A to be about 1.40 Å, the C–N linkages are shorter at 1.33 Å. The B-ring has longer C–C bonds. Ring D has the shortest bonds at r_{10} and r_{11}, 1.33 Å and the only other notable feature is that r_{14} is short, 1.30 Å. These data compare favorably with a number of crystal structures for dppz and substituted analogues. For the structure of $[Ru(bpy)_2(dmDPPZ)]^{2+}$, where dmDPPZ is 4,7-dimethyl-dppz[21] the general pattern of bond lengths is well reproduced including the shorter r_{14} relative to r_{15} and r_{13}. The main differences between the calculated structure and that observed in the crystal structure lie in the ABC ring systems. These rings are involved in the chelation to the metal. The bond angles are also in good agreement with the calculated structure varying +/− 2 degrees. Careful analysis of the dmDPPZ crystal structure reveals that it is quite distorted by the presence of the $[Ru(bpy)_2]^{2+}$ moiety. For the structure of $[PtCl_2(dppz)]$[22] those bonds close to the chelating Pt center do not show good correspondence with the calculated structure of dppz. However for r_8 to r_{15} the relative bond lengths are well predicted by calculation.

The optimized structure was used in the calculations of the vibrational frequencies. Importantly, the frequency calculations show no imaginary frequencies, consistent with a minimum energy geometry.

The calculated and observed frequencies and IR and Raman intensities for dppz and its deuterated analogues, in the 1000 to 1700 cm^{-1} region, are presented in Table 2. The Raman intensities are calculated from the Raman activity for 1064 nm excitation.[23] The spectra are shown in Figs. 2 and 3. The frequencies were scaled by 0.96 following the findings of Radom et al.[24]

In such a large molecule the normal modes are complex, involving the motion of many atoms in the structure. In order to better analyze this we calculated the percentage potential energy distributions (%PED) for the observed vibrational modes.[25] The mode distributions are parameterized in terms of bending

Table 2. Calculated and Experimental Wavenumbers and Intensities for dppz and its Isotopomers

ν[a]		dppz $\tilde{\nu}$/cm^{-1} (IR, R Int)[b]		d_4-dppz $\tilde{\nu}$/cm^{-1} (IR, R Int)		d_6-dppz $\tilde{\nu}$/cm^{-1} (IR, R Int)		d_{10}-dppz $\tilde{\nu}$/cm^{-1} (IR, R Int)		
		Calcd	Expt	Calcd	Expt	Calcd	Expt	Calcd	Expt	%PED[c]
80	b_2	1624 (3, 0)		1591 (6, 0)		1624 (4, 1)		1593 (3, 0)		E_H (20), DE_C(75)
79	b_2	1603 (18, 3)	1602 (16,25)	1605 (21, 2)	1601 (18,14)	1581 (59, 3)	1601 (53,3)	1580 (36, 2)	1580 (6,18)	A_H(20), A_C(75)
78	a_1	1593 (41, 27)	1586 (15,39)	1593 (51, 25)	1587 (24,52)	1569 (50, 48)	1576 (21,49)	1568 (51, 42)	1569 (39,64)	A_H(20), A_C(75)
77	b_2	1571 (13, 5)	1576 (18,12)	1569 (11, 6)	1571 (20,20)	1556 (18, 14)	1554 (81,19)	1554 (7, 13)		A_H (20), A_C(60), DE_C(10)
76	a_1	1568 (13, 4)		1562 (13, 4)		1557 (80, 3)		1545 (21, 2)	1546 (59,18)	A_H(10), E_H(10), A_C(30), DE_C(50)
75	a_1	1542 (0, 4)		1528 (1, 4)	1532 (4,20)	1523 (1, 7)		1512 (0, 5)	1516 (0,24)	A_H(15), E_H(15), A_C(35), DE_C(35)
74	b_2	1540 (7, 10)	1534 (3,17)	1539 (8, 10)		153 (64, 12)	1528 (26,30)	1532 (36, 10)	1532 (21,26)	A_C(10), DE_C(75)
73	a_1	1489 (72, 0)	1489 (100,4)	1470 (97, 11)	1476 (100,15)	1481 (67, 2)	1478 (100,5)	1443 (100, 8)	1445 (100,20)	A_H(10), E_H(35), A_C(15), DE_C(40)
72	b_2	1485 (7, 1)		1474 (3, 2)		1475 (2, 2)		1439 (1, 2)		A_H(20), E_H(15), A_C(20), DE_C(25)
71	a_1	1464 (14, 23)	1464 (10,24)	1438 (36, 7)	1438 (62,12)	1431 (89, 49)	1438 (54,29)	1414 (1, 37)		A_H(25), E_H(10), A_C(40), DE_C(15)
70	b_2	1463 (3, 0)		1439 (43, 0)		1403 (0, 1)		1393 (1, 0)		A_H(30), E_H(15), A_C(35), DE_C(15)
69	a_1	1419 (19, 4)	1431 (5,20)	1403 (0, 6)	1416 (12,40)	1368 (23, 62)	1384 (18,10)	1366 (24, 36)	1380 (18,22)	A_H(45) A_C(30), DE_C(15)
68	b_2	1414 (79, 2)	1414 (42,13)	1397 (75, 3)	1396 (52,0)	1350 (15, 0)		1315 (42, 1)	1314 (33,13)	A_H(50), E_H(10), A_C(30), DE_C(10)
67	a_1	1390 (0, 100)	1402 (5,100)	1389 (0, 100)	1393 (0,100)	1386 (2, 100)	1400 (5,100)	1385 (1, 100)	1402 (3,100)	A_C(15), DE_C(75)
66	a_1	1345 (100, 5)	1358 (55,4)	1343 (100, 9)	1355 (65,10)	1341 (49, 3)	1345 (77,7)	1299 (20, 5)	1284 (29,21)	A_H(10), E_H(5), A_C(5), DE_C(75)
65	a_1	1339 (0, 6)		1210 (1, 0)		1298 (71, 6)	1295 (76,3)	1254 (4, 4)		A_H(15), E_H(15), A_C(15), DE_C(40)
64	b_2	1336 (18, 2)	1338 (27,8)	1300 (7, 6)		1301 (36, 8)		1294 (0, 8)	1280 (0,20)	A_H(10), E_H(40), A_C(15), DE_C(20)
63	a_1	1330 (17, 24)	1321 (2,29)	1330 (29, 20)	1327 (8,29)	1255 (8, 4)	1264 (14,3)	1265 (86, 1)	1264 (81,14)	A_H(15), A_C(70), DE_C(10)
62	b_2	1297 (3, 4)		1255 (3, 0)		1284 (41, 2)		1244 (5, 0)		A_H(40), A_C(45)
61	b_2	1294 (6, 1)		1293 (9, 0)		1241 (0, 2)	1241 (14,0)	1211 (24, 5)	1215 (43,17)	A_H(15), A_C(55), DE_C (10)
60	a_1	1265 (1, 3)		1252 (11, 3)		1182 (12, 15)		1196 (3, 1)		A_H(10), A_C(70), DE_C(10)
59	a_1	1248 (4, 1)		1283 (22, 0)	1277 (19,4)	1234 (56, 1)	1219 (41,4)	1180 (5, 11)	1185 (25,25)	A_H (10), E_H(15), A_C(10), DE_C(65)
58	b_2	1231 (2, 1)	1230 (10,3)	1216 (0, 4)	1214 (4,18)	1196 (35, 4)	1196 (28,8)	1025 (2, 1)		E_H(50), A_C(10), DE_C(40)
57	b_2	1213 (0, 5)		1078 (5, 0)		1125 (7, 1)		1016 (1, 2)		A_H(20), E_H(10), A_C(35), DE_C(20)
56	a_1	1179 (6, 5)		1176 (4, 5)		1004 (0, 8)		1029 (43, 13)	1033 (72,26)	A_H(40), E_H(10), A_C(45)
55	a_1	1146 (1, 0)		1105 (10, 1)		1143 (17, 1)	1136 (28,3)			A_H(10), E_H(65), DE_C(20)
54	b_2	1127 (14, 1)	1136 (17,4)	1119 (21, 1)	1127 (25,6)					A_H(10), E_H(50), DE_C(35)
53	b_2	1116 (9, 0)	1123 (14,3)							A_H(55), A_C(35)
52	a_1	1103 (14, 2)	1106 (15,3)		1032 (100, 11)		1036 (97,16)			A_H(30), A_C(50), DE_C(20)
51	b_2	1076 (4, 0)		1027 (3, 1)		1017 (3, 3)				A_H(30), A_C(65)
50	a_1	1066 (36, 1)	1071 (44,3)	1065 (31, 0)	1072 (36,4)					A_H(30), A_C(40), DE_C(20)
49	a_1	1027 (26, 10)	1034 (34,16)	1025 (25, 12)	1025 (34,35)					A_C(65), DE_C(20)

a) Mode number and symmetry. b) Relative intensities for bands, normalized such that the most intense band in the reported spectral region is 100.
c) Potential energy distribution of normal mode of vibration, see text for details.

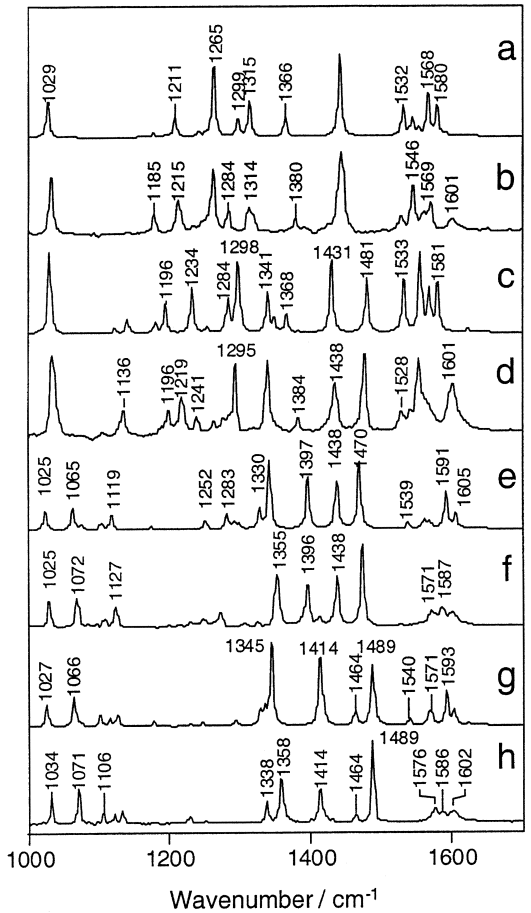

Fig. 2. Calculated and experimental IR spectra of dppz and its isotopomers. Calculated spectra of: d_{10}-dppz, trace a; d_6-dppz, trace c; d_4-dppz, trace e; dppz, trace g. Experimental spectra of: d_{10}-dppz, trace b; d_6-dppz, trace d; d_4-dppz, trace f; dppz, trace h. Experimental data were measured in $CHCl_3$.

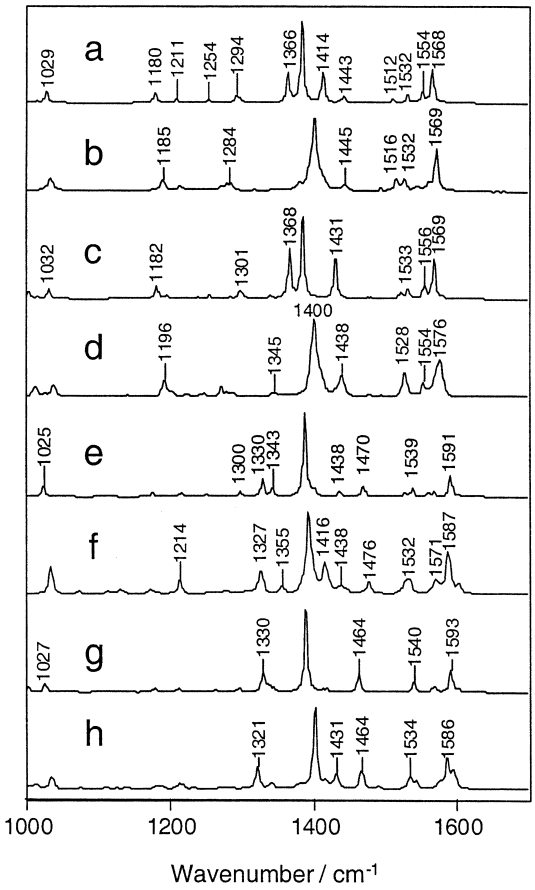

Fig. 3. Calculated and experimental Raman spectra of dppz and its isotopomers. Calculated spectra of: d_{10}-dppz, trace a; d_6-dppz, trace c; d_4-dppz, trace e; dppz, trace g. Experimental spectra of: d_{10}-dppz, trace b; d_6-dppz, trace d; d_4-dppz, trace f; dppz, trace h. Experimental data were measured on powder samples.

and stretching motions of CH at the A and B rings (A_H), CH at the E ring (E_H), CC at the AB rings (A_C), and CC at the DE rings (DE_C). In the region discussed there are no contributions from out-of-plane modes. Furthermore, in the 1000 to 1700 cm^{-1} region, deuteration results in significant mixing of modes such that the %PEDs differ significantly from one isotopomer to another. It is possible to compare the normal modes of the differing isotopomers quantitatively using available programs.[26] Such an analysis provides a method of tracking normal modes as they shift and alter their %PED with deuteration.

The IR spectra for dppz and its isotopomers are shown in Fig. 2. The spectrum of dppz shows 14 bands in the region of interest. These are clustered at 1000–1150, 1300–1500, and 1550–1610 cm^{-1}. The d_4-dppz spectrum shows a very similar pattern of bands at 1000–1150 and 1550–1610 cm^{-1} but a very different pattern is evident in the 1300–1500 cm^{-1} region. The pattern of shifts for d_6-dppz and d_{10}-dppz are complex across the entire region of interest. Nonetheless the close correspondence of the observed spectral features with the calculated frequencies and intensities permits assignments of the bands in the 1000–1700 cm^{-1} region.

The high frequency bands in the IR spectrum of dppz are also observed at similar wavenumber in the d_4-dppz spectrum. The normal modes assigned to these bands are modes 77–79. ν_{79} is localized on the ABC ring systems; it is therefore unsurprising that d_4-dppz substitution would have little effect on the wavenumber of this band. For d_6-dppz and d_{10}-dppz substitution perturbation of the transition wavenumber is predicted, shifting ν_{79} from 1603 to 1581, for d_6-dppz, and 1580 cm^{-1}, for d_{10}-dppz. The experimental spectra do not show this shift very clearly with a 1600 cm^{-1} band apparent in all four isotopomer spectra.

ν_{78} is also 90% ABC ring in nature. The pattern of isotope shifts predicted is similar to that for ν_{79}. ν_{78} is predicted to shift from 1593 cm^{-1} in dppz and d_4-dppz to 1569 cm^{-1} in d_6-dppz and 1568 cm^{-1} in d_{10}-dppz. This pattern is observed in the experimental data with the dppz and d_4-dppz spectra having bands at 1587 cm^{-1} which shift to 1570 cm^{-1} in the d_6-dppz and d_{10}-dppz spectra. ν_{77} appears at 1576 in dppz; it is predicted at 1571 cm^{-1}. This mode is strongly associated with the ABC-ring systems and does not shift from dppz to d_4-dppz. The band shifts significantly in d_6-dppz to 1554 $cm^{-1}$and it is predicted at 1556 cm^{-1}. For d_{10}-dppz no band is observed at

the predicted 1554 cm^{-1} but the calculation also predicts a drop of IR intensity for this transition and the activation of ν_{76} to IR activity which is consistent with the IR data.

In the 1300 to 1500 cm^{-1} region the pattern of isotope shifts is more complex. ν_{73} is correctly predicted at 1489 cm^{-1} for dppz. The normal mode for ν_{73} is DE ring based. d_4-dppz substitution is predicted to shift this mode to lower wavenumber (1470 cm^{-1}) and experimentally a band is observed at 1476 cm^{-1}. d_6-dppz substitution is predicted to have a smaller effect shifting the band to 1481 cm^{-1}; experimentally a band is observed at 1478 cm^{-1}. d_{10}-dppz substitution has a large effect shifting ν_{73} to 1445 cm^{-1}, it is predicted at 1443 cm^{-1}.

It is notable in the IR spectra of dppz and d_4-dppz that in the 1300 to 1500 cm^{-1} region the d_4-dppz spectrum has 4 strong bands whereas that of dppz shows only three. The band, which appears enhanced in intensity in the d_4-dppz spectrum, lies at 1438 cm^{-1} and is assigned as ν_{71}. The increased intensity is predicted to be about 50% that of the other 1300–1500 cm^{-1} bands. However the calculation also reveals that for d_4-dppz two bands, both IR allowed are present at 1439 and 1438 cm^{-1}. These are ν_{71} and ν_{70}, respectively, and their combined IR intensities result in the strong band observed at 1438 cm^{-1}.

ν_{68} is predicted and experimentally observed at 1414 cm^{-1} for dppz. This mode has significant A-ring character, mostly through C–H bending. d_4-dppz substitution shifts the band to 1396 cm^{-1}; the predicted value is 1397 cm^{-1}. d_6-dppz substitution is predicted to shift to 1350 cm^{-1} although no band is observed in this region. The calculation also predicts a drop in IR intensity for this mode. With d_{10}-dppz substitution ν_{68} is predicted at 1315 cm^{-1} and a band is observed at 1314 cm^{-1} in the experimental spectrum.

ν_{66} is observed at 1358 cm^{-1} and predicted at 1345 cm^{-1} as a strong IR band. This is best described as a DE-ring mode. Substitution at d_4-dppz results in a redistribution of potential energy to the A_H section of the molecule. However no appreciable shift is predicted or observed. For d_6-dppz a band is observed at 1345 cm^{-1} and predicted at 1341 cm^{-1}. For d_{10}-dppz also, the mode corresponding the ν_{66} is a mixture of a number of modes and it is predicted to show a very significant shift (-50 cm^{-1}) from dppz. The IR spectrum of d_{10}-dppz shows a band at 1284 cm^{-1} with reasonable IR intensity, as predicted.

In the lower frequency region 1000–1100 cm^{-1} two strong bands are observed for dppz; these correspond to ν_{49} and ν_{50} and they are ABC-ring modes. d_4- Deuteration has little effect on them but the spectra of d_6-dppz and d_{10}-dppz show shifts in wavenumber.

This analysis illustrates a number of points: (1) The agreement between the observed spectra and the calculations is good. (2) A number of the modes are localized on sections of the dppz framework. Indeed in the case of ν_{79} or ν_{49} the spectral isotope shifts are unambiguous in pointing to ABC-ring localized modes. (3) There are a large number of modes in this restricted spectral region but they can be predicted through calculation.

The Raman spectra of dppz and its isotopomers (Fig. 3) were collected on powdered samples and hence no depolarisation ratios were measured. Nevertheless the good correspondence between the observed bands and the calculated data make assignment relatively straightforward. The Raman spectra show relatively few strong bands in the 1100 to 1700 cm^{-1} region. A band at ca 1400 cm^{-1} dominates all four spectra. This is assigned as the ν_{67} mode. It is predicted to be the strongest band in this region and the mode is 75% DE ring stretch. Much of the energy of the mode is at the D-ring. For this reason the deuteration at either A,C or E rings has little effect on the wavenumber of the vibration or its predicted Raman intensity. Previous studies have assigned the 1407 cm^{-1} mode observed in dppz complexes to a phenazine-based vibration. The calculations presented herein suggest that to be too general a description.

In the higher wavenumber region, ν_{78} is observed in the spectra. This is an A-ring mode and shows the appropriate shifting pattern with isotope substitution. There is also a band at 1321 cm^{-1} in dppz assigned to ν_{63} and predicted at 1330 cm^{-1}. This mode is also strongly ABC-ring in nature showing little perturbation with d_4-dppz substitution, lying at 1327 cm^{-1} in the IR spectrum. There are significant shifts with d_6-dppz and d_{10}-dppz. For d_6-dppz and d_{10}-dppz, ν_{63} is observed at 1264 cm^{-1}. It is predicted to lie at 1255 cm^{-1} for d_6-dppz and 1265 cm^{-1} for d_{10}-dppz.

A number of studies have examined the resonance Raman spectra of complexes with dppz as a ligand. The vibrational analysis presented herein may provide some more insight into these previous studies.

The resonance Raman spectrum of the tris-chelate complex $[Ru(dppz)_3]^{2+}$ has been reported by McGarvey et al.[27] Their resonance excitation wavelength (457.9 nm) is coincident with the metal-to-ligand charge-transfer transition of the complex. The pattern of Raman band enhancements is informative as to the forces acting on the complex in the Franck-Condon region upon excitation.[28] As the resonance Raman enhancements for metal complexes are generally through A-term scattering only totally symmetric modes are enhanced.[29] The spectrum shows bands, with relative intensity in parentheses, at 1600(100), 1575(60), 1495(65), 1472(80), 1448(20), 1407(25), 1359(15), and 1311 cm^{-1} (35). These correspond to modes 78, 76, 73, 71, 69, 67, 66, and 63, respectively. Note that despite the fact that this is a metal complex the dppz bands are not shifted greater than 10 cm^{-1}. The very strong enhancement of modes 78 and 76 are indicative of an MLCT transition that places the excited electron into an MO on the dppz that perturbs the ABC-rings to a greater extent than D- or E-rings. It is interesting to note that the resonance Raman spectra of $[ReCl(CO)_3(dppz)]$ show rather different intensity patterns.[10] The spectrum at 457.9 nm, resonant with the MLCT transition, shows bands, with relative intensities, at 1598(23), 1577(8), 1495(62), 1473(31), 1447(50), 1406(100), and 1357 cm^{-1} (87). These correspond to modes 78, 76, 73, 71 , 69, 67, and 63, respectively. The much greater relative intensity for the ν_{67} mode suggests the charge-transfer in this case is further across the dppz structure towards the BDE-ring system.

The resonance Raman spectra of $[Ru(phen)_2(dppz)]^{2+}$ and $[Ru(phen)_2(d_6\text{-dppz})]^{2+}$ have also been reported.[27] This is interesting because it is the only example of vibrational spectral data on deuterated dppz complexes. The spectra were measured at 363.8 nm excitation, which corresponds to a mixture of MLCT and LC transitions. The spectra show a band at 1407 cm^{-1} in $[Ru(phen)_2(dppz)]^{2+}$ shifted to higher wavenumber

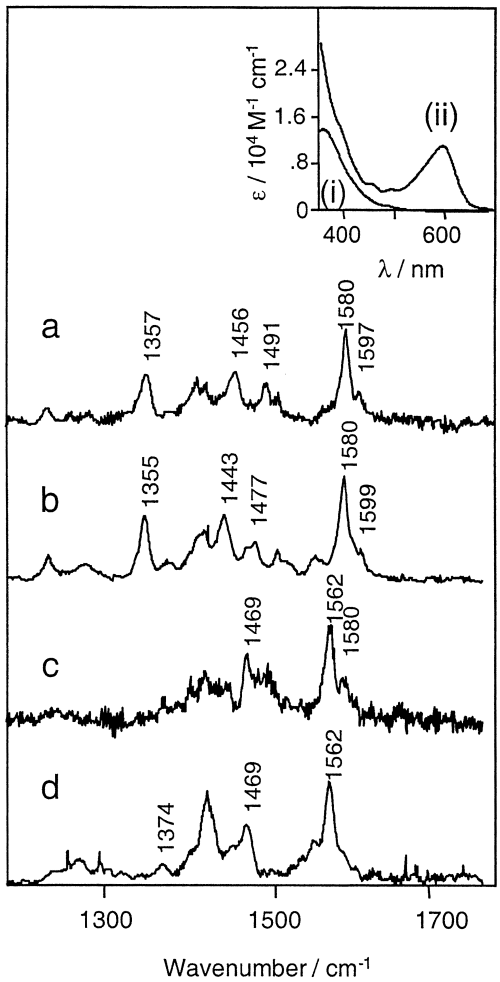

Fig. 4. Experimental resonance Raman spectra of: $[ReCl(CO)_3(dppz)]^-$ trace a; (b) $[ReCl(CO)_3(d_4\text{-dppz})]^-$ trace b; $[ReCl(CO)_3(d_6\text{-dppz})]^-$ trace c; $[ReCl(CO)_3(d_{10}\text{-dppz})]^-$ trace d, in CH_2Cl_2 solution. $\lambda_{exc} = 514.5$ nm. Inset: UV/visible spectra of $[ReCl(CO)_3(dppz)]$ in CH_2Cl_2 (i), and $[ReCl(CO)_3(dppz)]^-$ in CH_2Cl_2 (ii).

with deuteration. The authors note that the 1407 cm^{-1} band is proposed to be phenazine-based and thus a shift to higher frequency with d_6-dppz is surprising. Our calculations and Raman spectra show that the 1402 cm^{-1} is invariant with deuteration. It corresponds to mode 67, which is localized at the D-ring. One possible reason for the observed shift in this case is that the dppz ligand is spatially smaller in d_6-dppz at its chelating side. Thus it can interact more closely with the Ru centre resulting in the shift of the band.

Radical Anion: Spectra and Calculations. The resonance Raman spectra for the reduced complex $[ReCl(CO)_3(dppz)]^-$ and the deuterated analogues are shown in Fig. 4. The spectra, in the region 1200–1700 cm^{-1}, show two patterns; for $[ReCl(CO)_3(dppz)]^-$ and $[ReCl(CO)_3(d_4\text{-dppz})]^-$ there are strong bands at approximately 1580, 1456, and 1357 cm^{-1}, for $[ReCl(CO)_3(d_6\text{-dppz})]^-$ and $[ReCl(CO)_3(d_{10}\text{-dppz})]^-$ bands at approximately 1562 and 1469 cm^{-1} are present. The lower S:N ratio evident in the $[ReCl(CO)_3(d_6\text{-dppz})]^-$ spectrum is a consequence of emission from the sample. Attempts to generate spectra of the ligand anions failed due to strong emission backgrounds.

Previous studies on the Re(I) complexes suggest that the reduction of the complex is localized on the ligand and a radical anion is formed.[9] Furthermore the electrochemical data for such complexes suggest that the reducing electron occupies a redox MO polarized away from the metal centre, i.e. a phenazine based MO.[30] Hence the spectra observed in Fig. 4 are that of the radical anion $dppz^{\bullet -}$, and its isotopomers, enhanced through a radical anion π,π^* transition.

The structure and spectra of the radical anion may be modelled using ab initio calculations. The calculated (B3LYP/6-31G(d)) structural parameters for $dppz^{\bullet -}$ are listed in Table 1. The energy of the radical anion is ca 0.02 hartrees lower in energy than dppz. The $<s^2> = 0.7501$, is as expected for a radical anion species. The calculated structural data show an elongation of bonds at ring D, r_{10} and r_{11}, with contraction of r_9 and r_7 for $dppz^{\bullet -}$ realtive to dppz. The ϕ_{10}, ϕ_{11}, and ϕ_8 angles show significant perturbation. Most of the structural changes are at the D-ring and this is consistent with the population of a phenazine-based π^* MO as the redox orbital.[30]

The vibrational frequencies and intensities (IR and Raman) were obtained by calculation on the optimized geometry. Focusing on the spectral region 1250–1650 cm^{-1} approximately 13 modes show Raman activity. These are listed in Table 3. The experimental data set for the radical anion is restricted to the resonance Raman spectra from 1250–1650 cm^{-1} and our discussion is limited to that region. Attempts to generate IR spectra of the reduced complexes were unsuccessful due to the low solubility of the complexes in most solvents.

The modes calculated for the radical anion do not closely correspond with those of the neutral ligand. They can most usefully be grouped into phenanthroline-based and phenazine-based modes. The complex behavior of the normal modes is probably a consequence of the structural changes on going from neutral ligand to radical anion. In particular the B-ring is observed to contract whereas the D and E-rings expand and the A and C rings change rather little.

The calculated $dppz^{\bullet -}$ spectrum shows many more bands than are observed in the resonance Raman spectra of $[ReCl(CO)_3(dppz)]^-$ and the intensity patterns show little correlation between experimental and calculated spectra. However the experimental data pertains to a resonance Raman experiment in which the a_1 modes will be preferentially enhanced and the intensities will not correlate with the calculation.[31] This is exemplified by the resonance Raman spectrum of $[Ru(bpy)_2(dppz)]^{2+}$ [2] in which the ν_{67} mode which is the most intense Raman band is quite small in the resonance Raman spectrum. Importantly, the electronic properties of the complexes are not changed by deuteration thus the general pattern of intensity enhancements should be the same for each. A caveat to this is that if a band loses a great deal of Raman intensity upon deuteration, i.e. $(\delta\alpha/\delta q)_0$ is reduced, then the intensity in the resonance Raman spectra will also fall.[31]

Examination of the calculated $dppz^{\bullet -}$ data and the spectra of $[ReCl(CO)_3(dppz)]^-$ suggests that the band at 1580 cm^{-1} is ν_{80}. This is further supported by the prediction of a shift in ν_{80} for d_6-$dppz^{\bullet -}$ or d_{10}-$dppz^{\bullet -}$ but no shift with d_4-$dppz^{\bullet -}$. This pattern is observed in the spectra with the appearance of a band

Table 3. Calculated and Experimental Wavenumbers and Intensities for dppz$^{\bullet-}$ and its Isotopomers

ν[a]		dppz $\tilde{\nu}$/cm^{-1} (IR, R Int)[b]		d_4-dppz $\tilde{\nu}$/cm^{-1} (IR, R Int)		d_6-dppz $\tilde{\nu}$/cm^{-1} (IR, R Int)		d_{10}-dppz $\tilde{\nu}$/cm^{-1} (IR, R Int)		
		Calcd	Expt	Calcd	Expt	Calcd	Expt	Calcd	Expt	%PED[c]
80	a_1	1585 (1, 19)	1580 (—,100)	1585 (0, 21)	1580 (—,100)	1562 (8, 4)	1562 (—,100)	1551 (1, 25)	1562 (—,100)	A_H (20), A_C (65)
79	b_2	1584 (3, 55)	1597 (—,30)	1583 (2, 59)	1599 (—, 29)	1578 (2, 2)	1580 (—, 40)	1557 (1, 61)		A_H(20), A_C(65), DE_C(10)
78	b_2	1578 (3, 0)		1558 (15, 38)		1557 (0, 33)		1550 (9, 12)		E_H (20), A_C (10), DE_C (65)
77	a_1	1564 (8, 11)		1554 (4, 19)		1550 (0, 21)		1544 (4, 21)		E_H(20), A_C(20), DE_C(55)
76	b_2	1549 (10, 46)		1538 (0, 13)		1529 (12, 33)		1524 (6, 36)		A_H(20), A_C(75)
75	a_1	1536 (4, 18)		1514 (7, 31)		1522 (2, 9)		1500 (6, 20)		A_H(20), E_H(20), A_C(40), DE_C(20)
74	a_1	1490 (0, 25)	1491 (—,40)	1483 (1, 11)	1477 (—, 34)	1464 (0, 31)	1469 (—, 68)	1457 (0, 10)	1469 (—, 58)	A_H(20), E_H(10), A_C(50), DE_C(20)
73	b_2	1476 (5, 5)		1471 (3, 5)		1459 (1, 1)		1423 (1, 2)		A_H(35), E_H(10), A_C(30), DE_C(20)
72	a_1	1466 (0, 41)	1456 (—, 53)	1435 (2, 51)	1443 (—, 63)	1451 (0, 6)		1411 (0, 61)		A_H(20), E_H(25), A_C(15), DE_C(35)
71	b_2	1452 (1, 0)		1426 (13, 0)		1404 (0, 0)		1379 (1, 4)		A_H(30), E_H(10), A_C(30), DE_C(10)
70	b_2	1419 (15, 0)		1384 (3, 4)		1347 (14, 6)		1323 (3, 0)		A_H(30), E_H(10), A_C(30), DE_C(10)
69	a_1	1409 (2, 5)	1383 (5, 13)	1370 (1, 5)	1358 (0, 100)	1374 (—, 12)				A_H(40), E_H(10), A_C(15), DE_C(20)
68	a_1	1365 (1, 43)	1357 (—, 50)	1361 (0, 100)	1355 (—, 62)	1335 (16, 100)		1329 (0, 37)		A_H(5), A_C(40), DE_C(40)
67	a_1	1349 (12, 26)		1346 (4, 23)		1326 (27, 8)		1315 (100, 29)		A_H(25), A_C(45), DE_C(10)
66	b_2	1332 (1, 6)		1317 (20, 19)		1319 (6, 7)		1315 (28, 21)		A_H(25), E_H(20), A_C(30), DE_C(20)
65	a_1	1325 (45, 31)		1315 (64, 12)		1295 (100, 0)		1283 (53, 28)		A_C(10), DE_C(80)
64	b_2	1315 (26, 21)		1304 (7, 13)		1286 (24, 16)		1260 (17, 63)		A_H(10), A_C(60), DE_C(30)
63	a_1	1308 (100, 68)		1307 (100, 72)		1262 (4, 76)		1239 (6, 51)		A_C(10), DE_C(85)
62	b_2	1293 (5, 22)		1254 (20, 72)		1263 (3, 28)		1217 (6, 62)		A_H(25), E_H(20), A_C(25), DE_C(20)
61	a_1	1275 (19, 100)		1251 (6, 24)		1229 (8, 5)		1207 (3, 38)		E_H(10), A_C(10), DE_C(80)
60	b_2	1265 (13, 44)		1246 (14, 32)		1207 (10, 28)		1199 (3, 2)		A_H(10), E_H(20), A_C(10), DE_C(60)

a) Mode number and symmetry.
b) Relative intensities for bands, normalized such that the most intense band in the reported spectral region is 100.
c) Potential energy distribution of normal mode of vibration, see text for details.

at approximately 1562 cm^{-1} for [ReCl(CO)$_3$(d_6-dppz)]$^-$ and [ReCl(CO)$_3$(d_{10}-dppz)]$^-$. ν_{80} may be described as an ABC ring mode, it corresponds to ν_{78} of neutral dppz and is shifted down in frequency only slightly because the ABC-ring systems are not greatly perturbed by reduction of the ligand to dppz$^{\bullet-}$. The spectrum of [ReCl(CO)$_3$(dppz)]$^-$ also shows a band at 1491 cm^{-1}. This corresponds to ν_{74} in the calculated data. This mode is almost 70% AB ring in character. The mode is predicted to shift to lower wavenumber with deuteration, 1483 cm^{-1} for d_4-dppz$^{\bullet-}$, 1464 cm^{-1} for d_6-dppz$^{\bullet-}$ and 1457 cm^{-1} for d_{10}-dppz$^{\bullet-}$. In the spectra a band is observed at 1477 cm^{-1} in [ReCl(CO)$_3$(d_4-dppz)]$^-$ and 1469 cm^{-1} in [ReCl(CO)$_3$(d_6-dppz)]$^-$ and [ReCl(CO)$_3$(d_{10}-dppz)]$^-$.

The band at 1456 cm^{-1} in the spectrum of [ReCl(CO)$_3$(dppz)]$^-$ lies close to the predicted ν_{72} frequency (1466 cm^{-1}). The ν_{72} mode is a delocalized vibration. The 1456 cm^{-1} band is predicted to shift to 1435, 1451, and 1411 cm^{-1} for d_4-dppz$^{\bullet-}$, d_6-dppz$^{\bullet-}$, and d_{10}-dppz$^{\bullet-}$, respectively. The spectrum of [ReCl(CO)$_3$(d_4-dppz)]$^-$ has a band at 1443 cm^{-1}. No band is observed in this region for d_6-dppz$^{\bullet-}$ and in the spectrum of d_{10}-dppz$^{\bullet-}$ the solvent band at 1423 cm^{-1} obscures the region. The ν_{72} band of d_6-dppz$^{\bullet-}$ is predicted to have a lower relative intensity than for the other deuterated analogues, furthermore the low S:N ratio of the [ReCl(CO)$_3$(d_6-dppz)]$^-$ spectrum makes identification of such weak modes difficult. ν_{72} of dppz$^{\bullet-}$ corresponds to ν_{73} of dppz shifting down in frequency by about 20 cm^{-1}.

A strong band is observed at 1357 cm^{-1} in the spectrum of [ReCl(CO)$_3$(dppz)]$^-$ which we assign as ν_{68}, a delocalised mode (corresponding to ν_{67} of dppz). This shifts to 1355 cm^{-1} in the spectrum of [ReCl(CO)$_3$(d_4-dppz)]$^-$, as predicted. Neither the [ReCl(CO)$_3$(d_6-dppz)]$^-$ or [ReCl(CO)$_3$(d_{10}-dppz)]$^-$

spectra show any features in this region.

A number of studies have attempted to use resonance Raman spectroscopy to analyze the nature of the excited state in complexes containing dppz as a ligand. Turro et al.[2] used a single color pump-probe resonance Raman experiment to probe the excited state of $[Ru(phen)_2(dppz)]^{2+}$ with 355 nm excitation. They note the clear grow in of bands at 1365 and 1453 cm^{-1}. These correlate very well with the 1357 and 1456 cm^{-1} bands observed in the spectra of $[ReCl(CO)_3(dppz)]^-$. This suggests that the lowest excited state probed for $[Ru(phen)_2(dppz)]^{2+}$ contains a $dppz^{\bullet-}$ moiety and thus the excited state is MLCT in nature. This is in agreement with a number of studies on Ru(II) complexes with dppz.[8]

The excited state spectrum of $[Ru(phen)_2(dppz)]^{2+}$ has also been measured at 532, 396, and 321 nm.[27] With 532 nm excitation the 1458 and 1366 cm^{-1} bands are observed; however at 396 and 321 nm the pattern of intensities of the transient features are altered. Furthermore the transient resonance Raman spectrum of $[Ru(phen)_2(d_6\text{-dppz})]^{2+}$ shows no feature at 1366 cm^{-1} but a new band at 1316 cm^{-1}. The calculated spectrum of d_6-$dppz^{\bullet-}$ shows a band at 1335 cm^{-1} with a_1 symmetry that could correspond to ν_{68}. The correlation of transient vibrational spectroscopic data with $dppz^{\bullet-}$ provides further evidence of an MLCT excited state assignment.

There is significant interest in how excited state resonance Raman spectra of dppz complexes change with incorporation of the complexes into DNA. These calculations are insufficient to provide a detailed interpretative model of such interactions. However they provide an excellent basis for the development of $dppz^{\bullet-}$ modelling which incorporates solvent effects and H-bonding.

Conclusions

This paper has presented the vibrational spectra of dppz and its deuterated analogues as well as the resonance Raman spectra of $[ReCl(CO)_3(dppz)]^-$ and its deuterated isotopomers. Ab initio calculations on dppz are able to model the structure of the ligand. This predicted structure is similar to crystallographic data on complexes containing dppz and substituted dppz ligands. Furthermore frequency calculations on dppz and its isotopomers are able to predict the observed vibrational spectral properties. Analyses of these data reveal that the vibrational spectra of dppz contains normal modes that are vibrationally localized on sections of the ligand framework. Modes based over the phenanthroline and phenazine ring systems may be identified.

Resonance Raman data for Ru(II) and Re(I) complexes indicate the nature of the MLCT transition. In the case of Ru(II) complexes the strong enhancements of modes that are clearly phen-based in nature points to an acceptor MO in the MLCT transitions which is phen-based. This is not the case in the Re(I) complexes. There the strong relative enhancement of the phenazine-based 1406 cm^{-1} band suggests that the acceptor MO has much greater phenazine character.

The structure calculated for $dppz^{\bullet-}$ shows significant structural distortion at the BDE-rings. This is consistent with the population of an MO localized over those ring systems. The frequency calculations on $dppz^{\bullet-}$ show phen-based and phenazine-based modes, although the normal modes are quite different from the neutral molecule. The spectral features of $dppz^{\bullet-}$ have been characterised through the resonance Raman spectra of $[ReCl(CO)_3(dppz)]^-$. These spectra are dominated by phen-based modes of $dppz^{\bullet-}$. These same modes appear in the excited state resonance Raman spectra of Ru(II) complexes with dppz. This is consistent with the population of MLCT excited states in which the acceptor MO has considerable phenazine character.

Support from the New Zealand Lottery Commission and the University of Otago Research Committee (Grant number B01) for the purchase of the Raman spectrometer is gratefully acknowledged. A. F. thanks the Alliance Group Postgraduate Scholarship award.

References

1 A. Ambroise and B. G. Maiya, *Inorg. Chem.*, **39**, 4256 (2000); A. Ambroise and B. G. Maiya, *Inorg. Chem.*, **39**, 4264 (2000); F. M. O'Reilly and J. M. Kelly, *J. Phys. Chem. B*, **104**, 7206 (2000); O. Schiemann, N. J. Turro, and J. K. Barton, *J. Phys. Chem. B*, **104**, 7214 (2000); L. Flamigni, S. Encinas, F. Barigelletti, F. M. MacDonnell, K. J. Kim, F. Puntoriero, and S. Campagna, *Chem. Commun.*, **2000**, 1185; J. G. Liu, B. H. Ye, Q. L. Zhang, X. H. Zou, Q. X. Zhen, X. Tian, and L. N. Ji, *J. Biol. Inorg. Chem.*, **5**, 119 (2000); C. E. Keller, C. Pollard, L. K. Yeung, W. D. Plessinger, and C. J. Murphy, *Inorg. Chim. Acta*, **298**, 209 (2000); E. D. A. Stemp, R. E. Holmlin, and J. K. Barton, *Inorg. Chim. Acta*, **297**, 88 (2000); D. Ossipov, E. Zamaratski, and J. Chattopadhyaya, *Helv. Chim. Acta* , **82**, 2186 (1999); B. Onfelt, P. Lincoln, and B. Norden, *J. Am. Chem. Soc.*, **121**, 10846 (1999); C. M. Che, M. S. Yang, K. H. Wong, H. L. Chan, and W. Lam, *Chem.-Eur. J.*, **5**, 3350 (1999); S. A. Tysoe, R. Kopelman, and D. Schelzig, *Inorg. Chem.*, **38**, 5196 (1999); K. E. Erkkila, D. T. Odom, and J. K. Barton, *Chem. Rev.*, **99**, 2777 (1999).

2 W. Chen, C. Turro, L. A. Friedman, J. K. Barton, and N. J. Turro, *J. Phys. Chem. B*, **101**, 6995 (1997).

3 A. E. Friedman, J. -C. Chambron, J. -P. Sauvage, N. J. Turro, and J. K. Barton, *J. Am. Chem. Soc.*, **112**, 4960 (1990); C. Hiort, P. Lincoln, and B. Nordén, *J. Am. Chem. Soc.*, **115**, 3448 (1993); Y. Jenkins, A. E. Friedman, N. J. Turro, and J. K. Barton, *Biochemistry*, **31**, 10809 (1992); C. Turro, S. H. Bossmann, Y. Jenkins, J. Barton, and N. J. Turro, *J. Am. Chem. Soc.*, **117**, 9026 (1995).

4 J. R. Schoonover, G. F. Strouse, R. B. Dyer, W. D. Bates, P. Chen, and T. J. Meyer, *Inorg. Chem.*, **35**, 273 (1996).

5 B. Onfelt, P. Lincoln, B. Norden, J. S. Baskin, and A. H. Zewail, *Proc. Natl. Acad. Sci. U. S. A.*, **97**, 5708 (2000); E. J. C. Olson, D. Hu, A. Hormann, A. M. Jonkman, M. R. Arkin, E. D. A. Stemp, J. K. Barton, and P. F. Barbara, *J. Am. Chem. Soc.* **119**, 11458 (1997).

6 M. R. Waterland and K. C. Gordon, *J. Raman Spectrosc.*, **31**, 243 (2000).

7 A. C. Benniston, P. Matousek, and A.W. Parker, *J. Raman Spectrosc.* **31**, 503, (2000).

8 C. G. Coates, L. Jacquet, J. J. McGarvey, S. E. J. Bell, A. H. R. Al-Obaidi, and J. M. Kelly, *J. Am. Chem. Soc.*, **119**, 7130 (1997); J. J. McGarvey, P. Callaghan, C. G. Coates, J. R. Schoonover, J. M. Kelly, L. Jacquet, and K. C. Gordon, *J. Phys. Chem. B*, **102**, 5941 (1998).

9 M. R. Waterland, K. C. Gordon, J. J. McGarvey, and P. M.

Jayaweera, *J. Chem. Soc., Dalton Trans.*, **1998**, 609.

10 L. Ould-Moussa, O. Poizat, M. Castella-Ventura, G. Buntinx, and E. Kassab, *J. Phys. Chem.*, **100**, 2072 (1996).

11 T. Junk, W. J. Catallo, and J. Elguero, *Tet. Lett.*, **38**, 6309 (1997).

12 J. E. Dickeson and L. A. Summers, *Aus. J. Chem.*, **23**, 1023 (1970); R. D. Gillard, R. E. E. Hill, and R. Maskill, *J. Chem. Soc. A*, **1970**, 1447.

13 S. P. Schmidt, W. C. Trogler, and F. Basolo, *Inorg. Syn.*, **28**, 161 (1990).

14 J. V. Caspar and T. J. Meyer, *J. Phys. Chem.*, **87**, 952 (1983).

15 E. Wentrup-Byrne, C. A. Armstrong, R. S. Armstrong, and B. M. Collins, *J. Raman Spectrosc.*, **28**, 151 (1997).

16 T. J. Simpson and K. C. Gordon, *Inorg. Chem.*, **34**, 6323 (1995).

17 M. R. Waterland, T. J. Simpson, K. C. Gordon, and A. K. Burrell, *J. Chem. Soc., Dalton Trans.*, **1998**, 185.

18 M. J. Frisch, G. W. Trucks, H. B. Schlegel, G. E. Scuseria, M. A. Robb, J. R. Cheeseman, V. G. Zakrzewski, J. A. Montgomery, Jr., R. E. Stratmann, J. C. Burant, S. Dapprich, J. M. Millam, A. D. Daniels, K. N. Kudin, M. C. Strain, O. Farkas, J. Tomasi, V. Barone, M. Cossi, R. Cammi, B. Mennucci, C. Pomelli, C. Adamo, S. Clifford, J. Ochterski, G. A. Petersson, P. Y. Ayala, Q. Cui, K. Morokuma, D. K. Malick, A. D. Rabuck, K. Raghavachari, J. B. Foresman, J. Cioslowski, J. V. Ortiz, A. G. Baboul, B. B. Stefanov, G. Liu, A. Liashenko, P. Piskorz, I. Komaromi, R. Gomperts, R. L. Martin, D. J. Fox, T. Keith, M. A. Al-Laham, C. Y. Peng, A. Nanayakkara, C. Gonzalez, M. Challacombe, P. M. W. Gill, B. Johnson, W. Chen, M. W. Wong, J. L. Andres, C. Gonzalez, M. Head-Gordon, E. S. Replogle, and J. A. Pople, "Gaussian 98, Revision A.7," Gaussian, Inc., Pittsburgh PA (1998).

19 M. J. Frisch, G. W. Trucks, H. B. Schlegel, P. M. W. Gill, B. G. Johnson, M. A. Robb, J. R. Cheeseman, T. Keith, G. A. Petersson, J. A. Montgomery, K. Raghavachari, M. A. Al-Laham, V. G. Zakrzewski, J. V. Ortiz, J. B. Foresman, J. Cioslowski, B. B. Stefanov, A. Nanayakkara, M. Challacombe, C. Y. Peng, P. Y. Ayala, W. Chen, M. W. Wong, J. L. Andres, E. S. Replogle, R. Gomperts, R. L. Martin, D. J. Fox, J. S. Binkley, D. J. Defrees, J. Baker, J. P. Stewart, M. Head-Gordon, C. Gonzalez, and J. A. Pople, "Gaussian 94, Revision D.4," Gaussian, Inc., Pittsburgh PA, (1995).

20 G. Schaftenaar and J. H. Noordik, *J. Comput.-Aided Mol. Design*, **14**, 123 (2000).

21 N. Komatsuzaki, R. Katoh, Y. Himeda, H. Sugihara, H. Arakawa, and K. Kasuga, *J. Chem. Soc., Dalton Trans.*, **2000**, 3053.

22 A. Klein, T. Scheiring, and W. Kaim, *Z. Anorg. Allg. Chem.*, **625**, 1177 (1999).

23 G. A. Guirgis, Y. E. Nashed, and J. R. Durig, *Spectrochim. Acta Part A*, **56**, 1065 (2000).

24 A. P. Scott and L. Radom, *J. Phys. Chem.*, **100**, 16502 (1996).

25 G. Balakrishnan, P. Mohandas, and S. Umapathy, *Spectrochim. Acta Part A*, **53**, 1553 (1997).

26 A. K. Grafton and R. A. Wheeler, *Comp. Phys. Commun.*, **113**, 78 (1998); A. K. Grafton and R. A. Wheeler, *J. Comp. Chem.*, **19**, 1663 (1998).

27 C. G. Coates, J. J. McGarvey, J. M. Kelly, P. E. Kruger, and M. E. Higgins. *J. Raman Spectrosc.*, **31**, 283 (2000).

28 D. S. Egolf, M. R. Waterland, and A. Myers-Kelley, *J. Phys. Chem. B*, **104**, 10727 (2000).

29 R. J. H. Clark and T. J. Dines, *Angew. Chem., Int. Ed. Engl.*, **25**, 131 (1986).

30 J. Fees, W. Kaim, M. Moscherosch, W. Matheis, J. Klima, M. Krejcik, and S. Zalis, *Inorg. Chem.*, **32**, 166 (1993).

31 R. S. Czernuszewicz and T. G. Spiro in "Inorganic Electronic Structure and Spectroscopy," Vol. I,ed by E. I. Solomon and A. B. P Lever, John Wiley and Sons, Inc, New York (1999), p. 353.